Coarsening Foams Robustly Reach a Self-Similar Growth Regime

Jérôme Lambert,[1,*] Rajmund Mokso,[2] Isabelle Cantat,[1] Peter Cloetens,[2] James A. Glazier,[3] François Graner,[4,5] and Renaud Delannay[1]

[1]*IPR Université Rennes 1, UMR CNRS 6251, bâtiment 11a, Campus Beaulieu, 35042 Rennes Cedex, France*
[2]*X-ray Imaging Group–ESRF, BP 220, 38043 Grenoble Cedex 9, France*
[3]*Department of Physics, Swain Hall West 159, Indiana University, 727 East Third Street, Bloomington, Indiana 47405-7105, USA*
[4]*Spectrométrie Physique, Université Grenoble I, UMR CNRS 5588, 140 avenue de la Physique, BP 87, 38402 Martin d'Hères Cedex, France*
[5]*CNRS–Institut Curie, UMR 3215, 26 rue d'Ulm, 75248 Paris Cedex 05, France*

(Received 12 January 2009; revised manuscript received 13 November 2009; published 18 June 2010)

Dry liquid foams coarsen like other diphasic systems governed by interfacial energy: gas slowly diffuses across liquid films, resulting in large bubbles growing at the expense of smaller ones which eventually shrink and disappear. A foam scatters light very effectively, preventing direct optical observation of bubble sizes and shapes in large foams. Using high speed x-ray tomography, we have produced 4D movies (i.e., 3D + time) of up to 30 000 bubbles. After a transient regime, the successive images look alike, except that the average bubble size increases as the square root of time: This scaling state is the long sought self-similar growth regime. The bubble size and face-number distributions in this regime are compared with experimental distributions for grains in crystals and with numerical simulations of foams.

DOI: 10.1103/PhysRevLett.104.248304 PACS numbers: 82.70.Rr, 83.80.Iz

Diphasic systems governed by interfacial energy, like dispersed emulsions, grains in polycrystals and foams, coarsen. The dispersed phase diffuses through the continuous one to reduce the total area of interface. On average, large domains, which have lower pressure, expand at the expense of smaller ones that shrink and eventually disappear one by one. Hence the number of domains steadily decreases and the average size of the remaining domains increases.

For very dilute emulsions, domains are separated spheres entirely characterized by their radii. Their coarsening dynamics is known as "Ostwald ripening" or "LSW" after Lifshitz, Slyosov, and Wagner [1–3]. At long times, the distribution of domain volumes relative to their average $V/\langle V(t)\rangle_{\mathrm{WS}}$ reaches a universal distribution, independent of the initial one, where $\langle\cdot\rangle_{\mathrm{WS}}$ designates an average over the whole set of domains. After a transient, the growth regime becomes self-similar. The statistical distributions of topological and dimensionless geometrical quantities remain invariant in time while the characteristic scales continue to increase. As a consequence, the local diffusion law [2,3] implies that $\langle V(t)\rangle_{\mathrm{WS}} \sim t$.

In the opposite limit, for a dry diphasic system, the continuous matrix occupies a much smaller volume than the dispersed phase and domains resemble closely packed polyhedra (see Fig. 1). Dry diphasics include concentrated emulsions, grains in crystals, and "dry" liquid foams with low (typically $<5\%$) water volume fractions [4]. In dry diphasics diffusion takes place through thin walls of roughly constant thickness. In 2D, the growth rate of each domain depends only on its number of neighbors, not on its size (von Neumann's law [5]). 2D self-similar growth has been observed experimentally and in simulations [6]. 3D growth is difficult to analyze theoretically, since the growth rate of a 3D bubble depends in a complex way on its size and shape [7,8]. Many numerical simulations have sought the self-similar growth regime in 3D [9–15]. 3D experiments are difficult. Grains in crystals are hard to follow in real time [16–18]. In dry foams, most of the liquid accumulates at the junctions of thin films, forming a continuous network of liquid channels called Plateau borders [4] (Fig. 1). Films and Plateau borders absorb light weakly but diffract it strongly, making the structure difficult to image. Thus observed signatures of a self-similar growth have been indirect [19,20]. Magnetic-resonance imaging (MRI) [21,22] and optical tomography [23] experiments have visualized the evolution of the Plateau borders in liquid foams, with 200 and 48 bubbles, respectively, too few to establish whether the coarsening regime is self-similar, which requires at least several thousand bubbles at each sampling time to compute meaningful

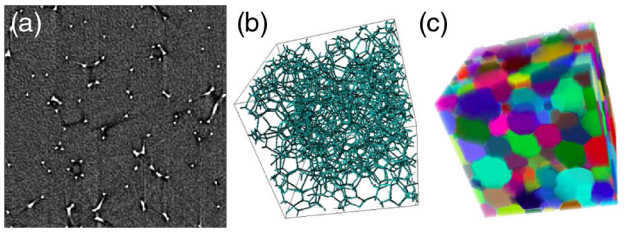

FIG. 1 (color online). (a) 300 × 300 pixels (2.25 × 2.25 mm^3) 2D gray-scale cut extracted from a complete 3D raw image of a dry liquid foam. (b) 3D view of a binary reduction of the same 3D foam image. (c) Image with individual bubbles color coded.

statistics [12]. In this Letter, we determine experimentally the distribution of bubble sizes and face numbers for such a foam: we show that, at long times, they remain constant, proving that 3D dry foams reach a self-similar growth regime. Because foams are a good model of generic diphasic growth, our results suggest that other diphasic materials which coarsen due to interfacial energy should also reach self-similar growth regimes.

Our optimized tomography technique based on [24] achieves 4×10^9 voxel images (with a 7.5 μm voxel linear dimension) of dry foams within 30 s using the FReLoN camera devised at ESRF. The acquisition time is much faster than the characteristic coarsening time, itself much smaller than the total duration of the experiment. The sample cell is a Plexiglas cylinder: 15 mm in outer diameter, with a subregion of 7.5 mm height in the x-ray beam, and a wall thickness of 0.5 mm. Most of our measurements used a dry dishwashing liquid foam (hereafter foam 1), which we observed beginning at $t = 30$ min after foam fabrication until $t = 1100$ min. The foaming solution consists of distilled water, 4% commercial dishwashing liquid (Dreft, Procter & Gamble), and traces of C_6F_{14} to slow down coarsening. We form the foam using a commercial kitchen foamer, then transfer it to the sample cell being careful not to introduce large gaps or bubbles. Drainage during the first half-hour after foam fabrication induces bubble motion, preventing imaging for $t <$ 30 min. To reduce the liquid fraction and keep it uniform and stable throughout the duration of our experiments, we applied a negative pressure difference to the foam via porous plates at the bottom of the experimental cell. As in [24], we verified that bubble coalescence was negligible. We also measured distributions for another sample produced the same way (foam 2) and shaving foam (foam 3) produced using a commercial aerosol device (Gillette).

We segmented and analyzed the images using the APHELION software package following the procedures in [24]. Figure 1 shows different views of foam 1 at $t =$ 100 min. The Plateau borders are clearly resolved as seen in Fig. 1(a), which shows a 2.25×2.25 mm^2 gray-scale slice of height 7.5 μm. The films, which are smaller than the pixel size, are invisible, indicating that their liquid content is negligible compared to that of the Plateau borders. The liquid fraction is thus approximately the fraction of water containing voxels in the binary reduction of the raw image [see Fig. 1(b)], which preserves only the Plateau border mesh. For all samples and observation times, the measured fluid volume fraction is $2.0\% \pm 0.5\%$. Using a custom-written 3D image analysis toolkit, we approximated each bubble's faces by planar plaquettes. Since the curvature of the films is small, approximating the faces as flat introduces an error in the estimated volume of less than 5% for most bubbles. Figure 1(c) shows color-coded individual bubbles. We estimate the volume V and number of faces F for each bubble.

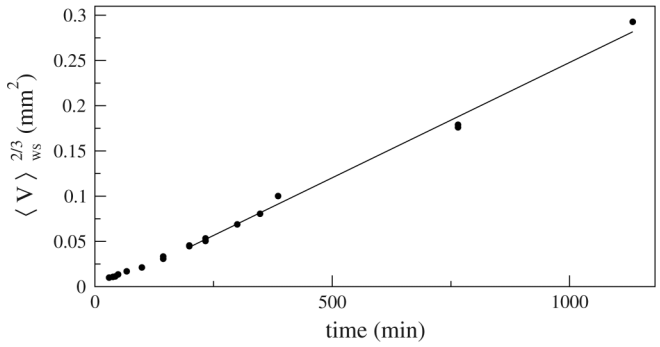

FIG. 2. $\langle V \rangle_{WS}^{2/3}$ vs time for foam 1 (points). Linear fit to experimental data for $t > 250$ min, corresponding to the self-similar growth regime (solid line).

In each successive image, we extract and analyze bubbles in a characteristic subregion of the sample cell, avoiding the cell walls. Computer capacity limits the number of analyzed bubbles at early stages and sample size at later stages. Figure 2 shows the average bubble volume as a function of time for foam 1. We plot $\langle V(t) \rangle_{WS}^{2/3}$ vs time to emphasize its linearity at long times. Dimensional arguments based on the local diffusion law [25,26] show that self-similar growth in dry foams implies that $\langle V(t) \rangle_{WS}^{2/3} \sim t$ [19,20] as we observe. However, the converse need not hold. Recall that for Oswald ripening, $\langle V(t) \rangle_{WS} \sim t$ [25].

We can measure bubble volumes ranging from a few voxels to the sample size. To compute comparable distributions at various times, we must apply upper and lower volume cutoffs scaled consistently with the average bubble volume. At early times, the lower cutoff eliminates small artifactual bubbles created by the image analysis software. We set the lower cutoff volume to $V_\epsilon = \langle V(t) \rangle_{WS}/120$, which coincides with a few voxels at $t = 30$ min. We adjust our analyzed subregion so that it always contains around 3000 bubbles with volumes larger than V_ϵ (except for $t =$ 1133 min when only 1700 bubbles remain). Averages denoted $\langle \cdot \rangle$ and the distributions which we present in the remainder of this Letter include only bubbles with volumes larger than the lower cutoff which are fully embedded in the subregion and do not touch its walls.

Figure 3 shows the distributions of the nondimensional length $\ell^* = V^{1/3}/\langle V(t)^{1/3} \rangle$ and of the number of faces per bubble for foam 1 for 7 times between $t = 30'$ and $t =$ $765'$. After a transient, the distributions stabilize. The length distribution differs from that calculated analytically for a dilute emulsion according to the LSW theory as shown in Fig. 3(a). It agrees reasonably well with distributions obtained with various simulations and experimental observations of normal grain growth, even if all these data lie outside our error bars [see Fig. 3(a)] The same observation is made for the face-number distributions [Fig. 3(b)]. The agreement with the lognormal distribution found in [9,17,27] is better for the face-number distribution [Fig. 4(b)] than for the length distribution [Fig. 4(a)].

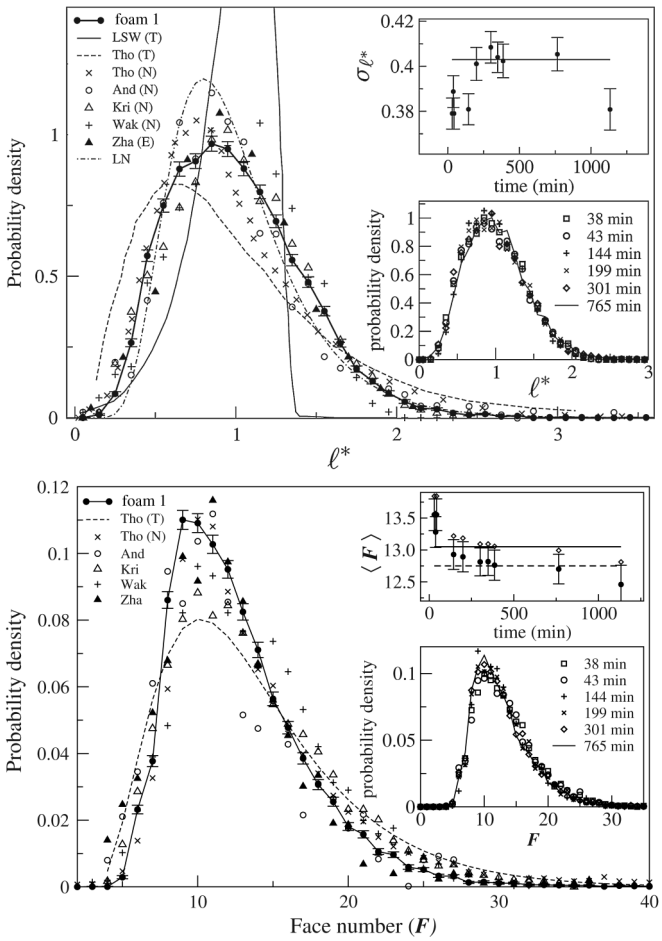

FIG. 3. (a) Probability density of the nondimensional length ℓ^* averaged over $t = 301$, 348, 386, 765, and 1133 min in the self-similar growth regime. We plot the lognormal distribution (LN) with first and second moments matching the experimental averages. We also show a variety of theoretical results (T) [2,3,12], simulation distribution results (N) [9–12] and an experimental distribution (E) for crystal grains obtained by serial sectioning [27]. Upper inset: $\sigma_{\ell^*} = \sqrt{\langle(\ell^* - 1)^2\rangle}$ vs t. The line is a guide for the eye at $\sigma_{\ell^*} = 0.402$. Lower inset: ℓ^* distributions in the transient regime. The distribution at $t = 765$ min is given as a reference. (b) Probability density of face numbers for the same samples. Upper inset: $\langle F \rangle$ vs t, raw data (solid symbols) and unbiased data (open symbols, see text). The horizontal lines are at $\langle F \rangle = 12.75$ and $\langle F \rangle_{\mathrm{UB}} = 13.05$. Lower inset: F distributions in the transient regime, for the same times as in (a).

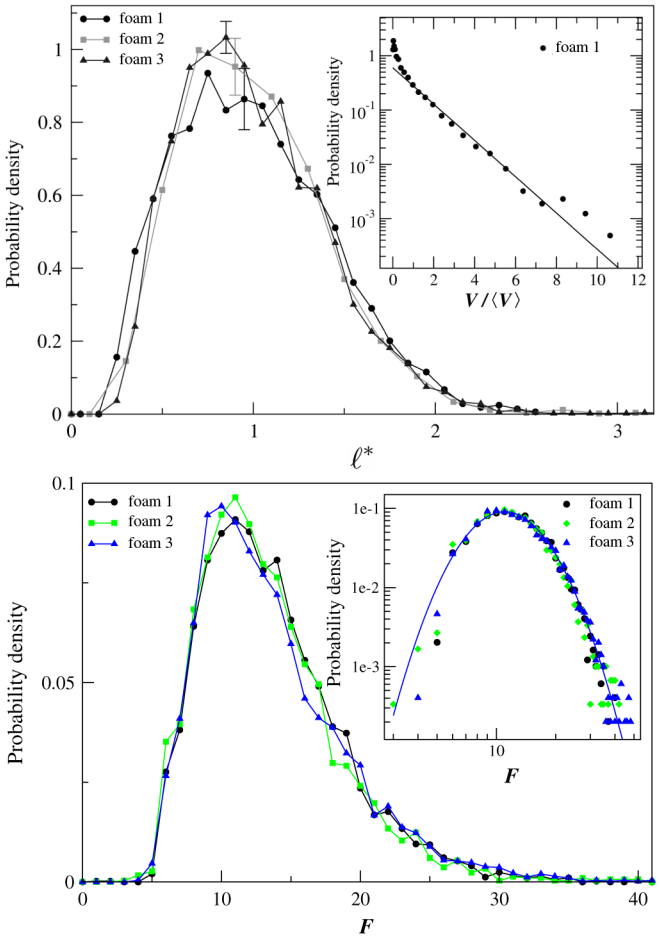

FIG. 4 (color online). (a) Probability density of ℓ^* for foam 1 (4931 bubbles in the sample), foam 2 (dishwashing liquid, 2986 bubbles, $t = 540$ min), foam 3 (shaving foam, 4957 bubbles, $t = 1440$ min) in the self-similar regime. Inset: lin-log plot of the probability density of the bubble volume (foam 1). The line shows a least square fit to exponential decay. (b) Probability density of the face number for the same samples at the same times. Inset: log-log plot of the same data. The line shows a least-squares fit to a parabola.

The evolution of the standard deviation of the ℓ^* distribution and the average number of faces $\langle F \rangle$ [Figs. 3(a) and 3(b) upper insets] show that the transient regime lasts about 200 min. The lower insets in Figs. 3(a) and 3(b) show the distributions in the transient regime. The steady state lasts from $t = 200$ min to $t = 800$ min, during which the average volume of the bubbles increases by a factor of 10.

The average volume $\langle V \rangle_F$ of sets of bubbles sharing the same F correlates with F (data not shown). For large F, $\langle V \rangle_F \propto F^{(2.5 \pm 0.3)}$, which is compatible with the exponent 2.25 observed in simulations [12,28].

For a given foam image, the errors due to imaging, image processing, and analysis produce error bars smaller than the size of the symbols in the plot of the distributions [Figs. 3(a) and 3(b)]. The plotted error bars represent expected statistical fluctuations due to counting error, estimated as follows: the error bars Δy drawn for a point at position (x, y) on a graph are $\Delta y = \pm y/\sqrt{n}$, where n is the number of bubbles analyzed at that time point. In the self-similar growth regime, $\sigma_{\ell^*} = 0.40 \pm 1\%$ and $\langle F \rangle = 12.7 \pm 1\%$. These fluctuations lie within the expected statistical fluctuation due to counting error of $1/\sqrt{3000} = 1.8\%$, except for the last point ($t = 1133$ min).

The finite size of the sample suppresses contributions of bubbles with volumes more than a few % of the volume of the analyzed subregion, creating a statistical bias, since a bubble's center cannot be closer than $V^{1/3}/2$ to the box

boundary [29,30]. We estimate the unbiased (UB) value of $\langle F\rangle$ analytically by assuming that the volume distribution takes the form $P(V) = \exp-[V/\langle V\rangle_{\mathrm{WS}}]/\langle V\rangle_{\mathrm{WS}}$ (see Fig. 4, inset), extrapolating to $V \to \infty$ and using the relation $\langle F\rangle_V = 14.57(V/\langle V\rangle_{\mathrm{WS}})^{0.3}$ obtained by averaging the experimental values. We find $\langle F\rangle_{\mathrm{UB}} = \langle F\rangle + 4.2/N^{1/3}$, to leading order in $1/N$, where N is the number of bubbles in the sample subregion. $\langle F\rangle_{\mathrm{UB}} = 13.05$ in the self-similar growth regime [Fig. 3(b), upper inset]. The correction computed for σ_{ℓ^*}, of the order of $0.1/N^{1/3}$, is negligible. The corrections to the distributions are small in comparison with the statistical noise.

Foams 2 and 3, for which we do not have data in the transient regime, have the same distributions as foam 1. The foams differ in their preparation and chemical composition [foam 2 (dishwashing liquid) and foam 3 (shaving foam)], so they also differ in their local diffusion coefficients controlling the gas flux through their thin films. This parameter is 8 times smaller in the shaving foam than in the dishwashing liquid foams. Nevertheless, their distributions are the same within error, as shown in Fig. 4. Thus the self-similar regime distributions are robust to differences in preparation and material parameters. In addition, the curves shown in the inset of Figs. 4(a) and 4(b) (close to linear and parabolic, respectively) are similar to those provided by theory and simulations (Fig. 13 and the inset of Fig. 19 of [12]). This agreement is compatible with the hypothesis that the growth of foam is self-similar, universal, and robust.

Because the transient regime is brief, many industrial foams should be in the self-similar regime during their use. The distributions we provide allow us to infer the statistical properties of a foam from the average volume, which can be easily measured. These distributions may also serve as inputs for more realistic numerical simulations, e.g., of foam's properties.

We thank the ESRF, D. Guillotin who built the experimental cells, L. Oger for his help on images processing, G. Thomas and R. de Almeida for discussions, and J. Émile for assistance during the experiments.

*jerome.lambert@univ-rennes1.fr

[1] W. Ostwald, *Grundriss der Allgem. Chemie* (Macmillan, London, 1908), p. 96; *Foundations of Analytic Chemistry* (Macmillan, London, 1908), 3rd English ed., p. 22; *Principles of Inorganic Chemistry* (Macmillan, London, 1902), p. 58.
[2] I. M. Lifschitz and V. V. Slyozov, Zh. Eksp. Teor. Fiz. **35**, 479 (1958) [Sov. Phys. JETP **8**, 331 (1959)].
[3] C. Wagner, Z. Elektrochem. **65**, 581 (1961).
[4] D. Weaire and S. Hutzler, *The Physics of Foams* (Oxford Univ. Press, Oxford, 2000).
[5] J. von Neumann, in *Metal Interfaces* (American Society for Metals, Cleveland, 1952), p. 108.
[6] J. Stavans, Rep. Prog. Phys. **56**, 733 (1993).
[7] W. W. Mullins, Acta Metall. **37**, 2979 (1989).
[8] R. MacPherson and D. Srolovitz, Nature (London) **446**, 1053 (2007).
[9] M. P. Anderson, G. S. Grest, and D. J. Srolovitz, Philos. Mag. B **59**, 293 (1989).
[10] F. Wakai, N. Enomoto, and H. Ogawa, Acta Mater. **48**, 1297 (2000).
[11] C. E. Krill III and L.-Q. Chen, Acta Mater. **50**, 3057 (2002).
[12] G. L. Thomas, R. M. C. de Almeida, and F. Graner, Phys. Rev. E **74**, 021407 (2006).
[13] D. Zöllner and P. Streitenberger, Scr. Mater. **54**, 1697 (2006).
[14] P. Streitenberger and D. Zöllner, Scr. Mater. **55**, 461 (2006).
[15] S. Jurine, S. Cox, and F. Graner, in *Proceedings of the 5th European Conference on Foams, Emulsions, and Applications, EUFOAM 2004 (Marne La Vallée, 5-8 July 2004)*, edited by M. Vignes-Adler, D. Weaire, and R. Miller [Colloids Surf. A **263**, 18 (2005)].
[16] W. M. Williams and C. S. Smith, J. Met. **4**, 755 (1952).
[17] F. N. Rhines and B. R. Patterson, Metall. Trans. A **13**, 985 (1982).
[18] K. M. Döbrich, C. Rau, and C. E. Krill, III, Metall. Mater. Trans. A **35**, 1953 (2004).
[19] D. J. Durian, D. A. Weitz, and D. J. Pine, Phys. Rev. A **44**, R7902 (1991).
[20] N. Mujica and S. Fauve, Phys. Rev. E **66**, 021404 (2002).
[21] C. Gonatas, J. Leigh, A. Yodh, J. Glazier, and B. Prause, Phys. Rev. Lett. **75**, 573 (1995).
[22] B. Prause and J. A. Glazier, in *Proceedings of the 5th Experimental Chaos Conference Orlando, Florida, 1999*, edited by M. Ding, W. L. Ditto, L. M. Pecora, and M. L. Spano (World Scientific, Singapore, 2001), pp. 427–436.
[23] C. Monnereau and M. Vignes-Adler, Phys. Rev. Lett. **80**, 5228 (1998).
[24] J. Lambert *et al.*, Phys. Rev. Lett. **99**, 058304 (2007).
[25] W. W. Mullins, J. Appl. Phys. **59**, 1341 (1986).
[26] J. A. Glazier and B. Prause, in *Foams, Emulsion and Their Applications: Proceedings of the Eurofoam Conference, Delft 2002*, edited by P. Zitha (Verlag MIT, Bremen, 2000), p. 120.
[27] C. Zhang, A. Suzuki, T. Ishimaru, and M. Enomoto, Metall. Mater. Trans. A **35**, 1927 (2004).
[28] A. M. Kraynik, D. A. Reinelt, and F. van Swol, Phys. Rev. Lett. **93**, 208301 (2004).
[29] C. Lantuéjoul, Microscopica Acta **5**, 266 (1980).
[30] R. E. Miles, in *Harding*, edited by E. F. and D. G. Kendall, Stochastic Geometry Vol. 202 (Wiley, New York, 1974).